Contents of this file

1. Figures S1 to S8

Introduction Figure S1 shows winter mixed layer depth anomalies using Argo data for comparison to Figure 1. Figures S2 and S3 included in the supporting information provide additional information on how the subantarctic water pools of the Central and Eastern Pacific are identified. Figures S4 and S5 show the raw adjoint sensitivities of volume to surface heat flux for the Central and Eastern adjoint sensitivity target regions. Figures S6 and S7 show the impacts of surface heat flux for the Central and Eastern adjoint sensitivity target regions for a longer time series than included in the main paper. Figure S8 shows that heat flux is the dominant control on the volume of the Central and Eastern adjoint sensitivity target regions.

Figures S1 - S8.

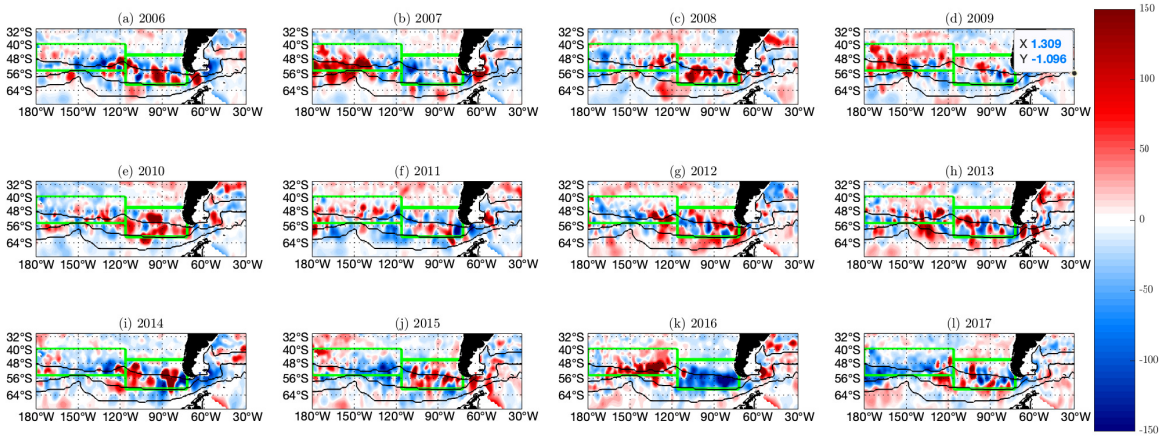

Figure S1. Winter mixed layer depth anomalies (m) for years (a) 2006 - (l) 2017 from Argo data. Green boxes show the central and eastern mode water formation pools. Black contours show sea surface height proxies(0.25, 1.0, 1.5 m) for the fronts of the Antarctic circumpolar current.

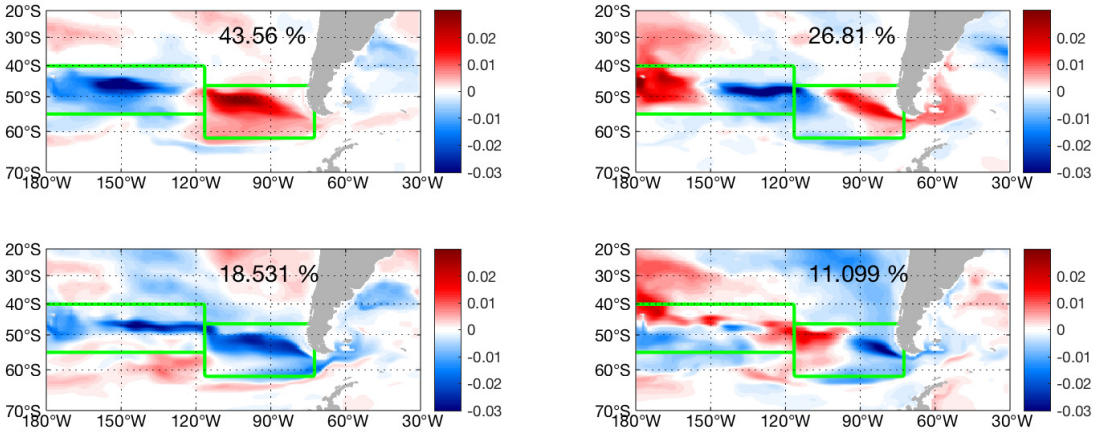

Figure S2. (a) First EOF of mixed layer depth in winters (JAS) for years 2006 -2017. (b) Second EOF, (c) Third EOF. (d) Fourth EOF. Green contours show the Central and Eastern control volumes. Percentages given are the percentage of variance explained by each EOF.

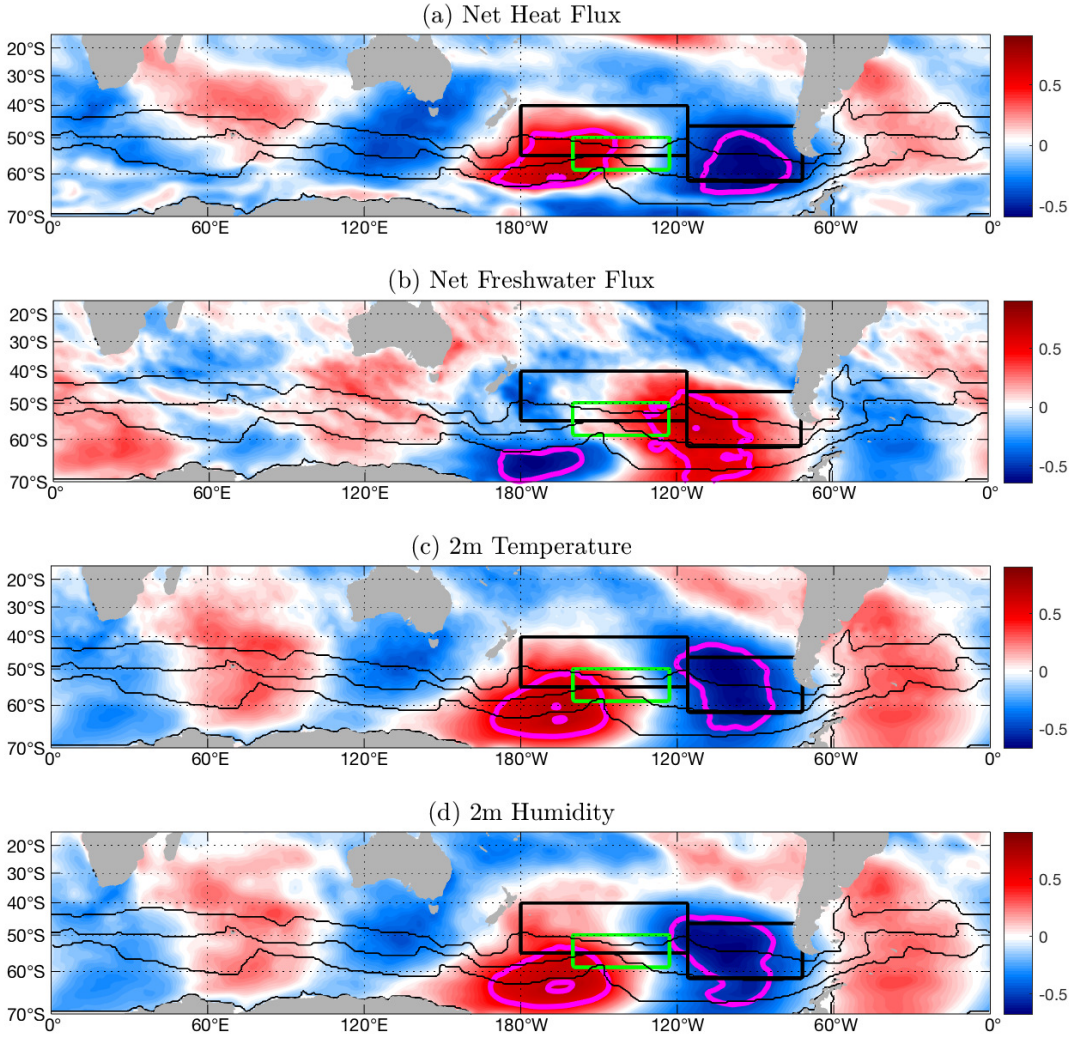

Figure S3. (a) Regression of mean sea level pressure within green contour with winter net heat flux (W m^{-2}). Magenta contours show areas of statistical significance. Green contour shows area of largest standard deviation of mean sea level pressure. Black boxes show central and eastern control volumes. Black contours show sea surface height (-0.25, -1, -1.5 m) which is used as a proxy for the fronts of the ACC. (b) Regression of mean sea level pressure within green contour with winter net freshwater flux (m s^{-1}). (c) Regression of mean sea level pressure within green contour with winter 2m temperature ($^{\circ}$ K). (d) Regression of mean sea level pressure within green contour with winter 2m humidity (kg kg^{-1}).

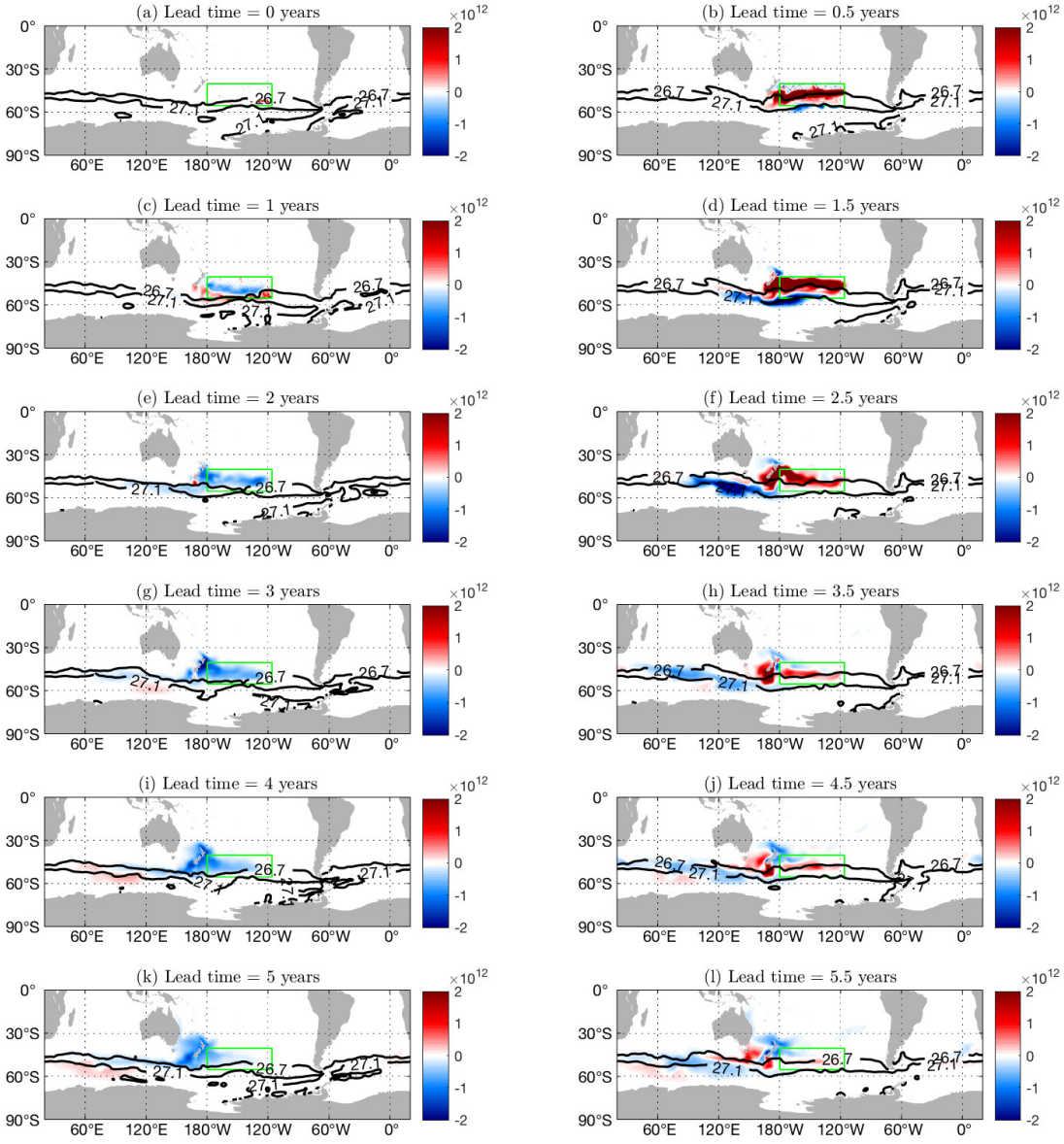

Figure S4. Sensitivity of volume to surface heat flux ($(m^3)/(W\ m^{-2})$) at the surface for lead times of 0 - 5.5 years. The Central adjoint sensitivity target region (green) and the outcrops of the bounding density surfaces (26.7 and 27.1 kg m^{-3}, black contours) are included.

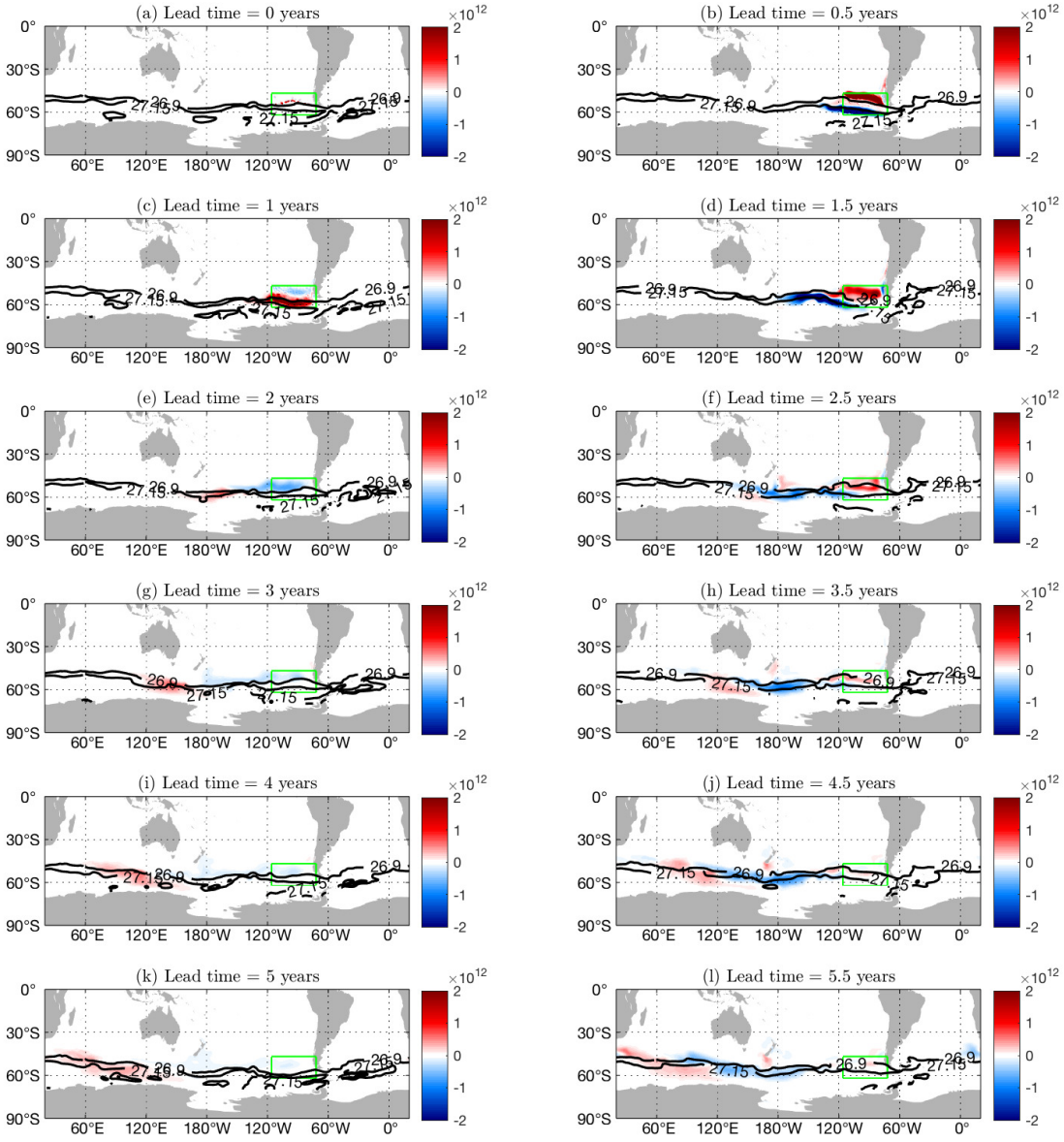

Figure S5. Sensitivity of volume to surface heat flux ($(m^3)/(W\ m^{-2})$) at the surface for lead times of 0 - 5.5 years. The Eastern adjoint sensitivity target region (green) and the outcrops of the bounding density surfaces (26.9 and 27.15 kg m^{-3}, black contours) are included.

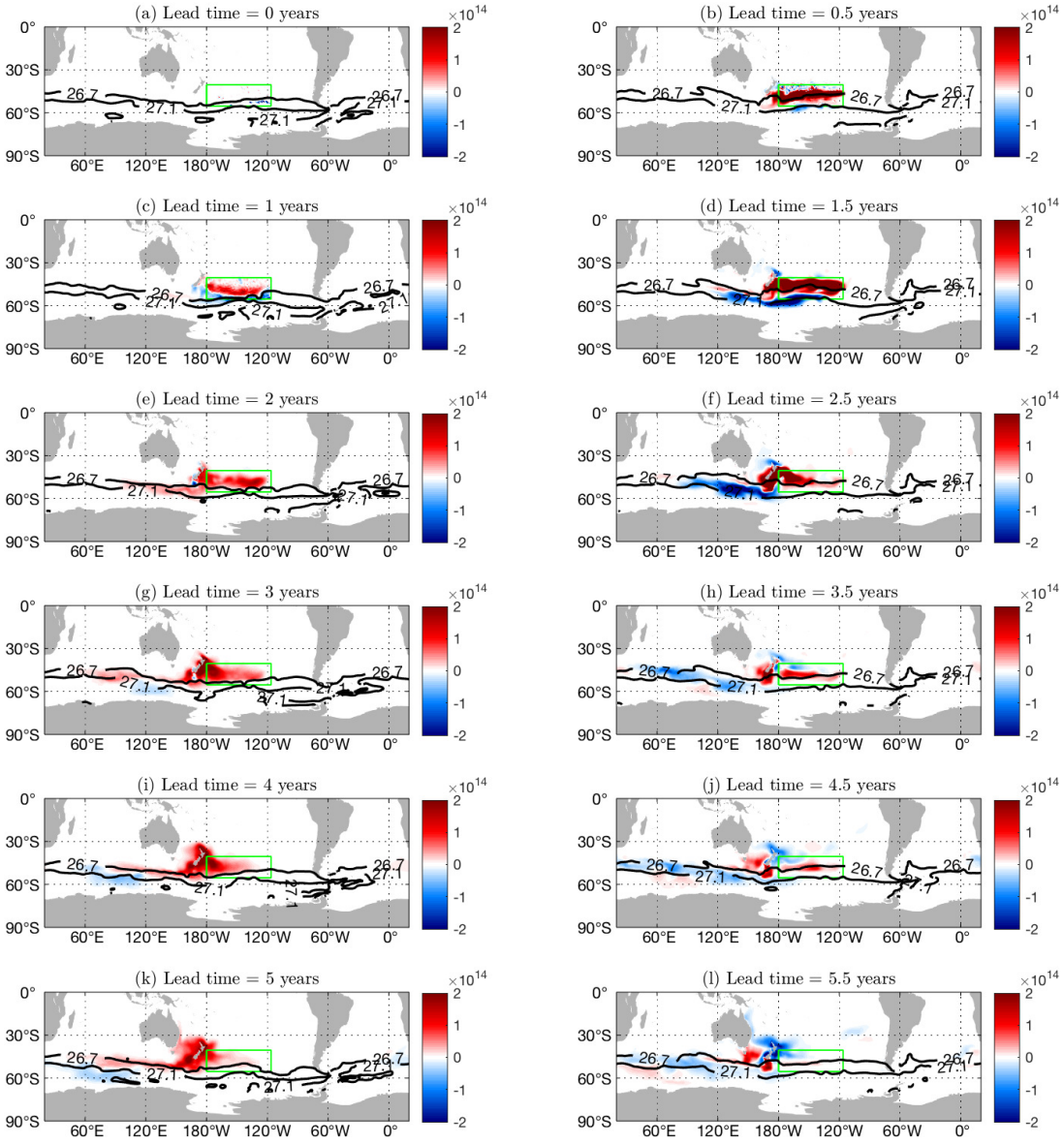

Figure S6. Surface heat flux impacts (m^3) at the surface for lead times of 0 - 5.5 years. The Central adjoint sensitivity target region (green) and the outcrops of the bounding density surfaces (26.7 and 27.1 kg m^{-3}, black contours) are included.

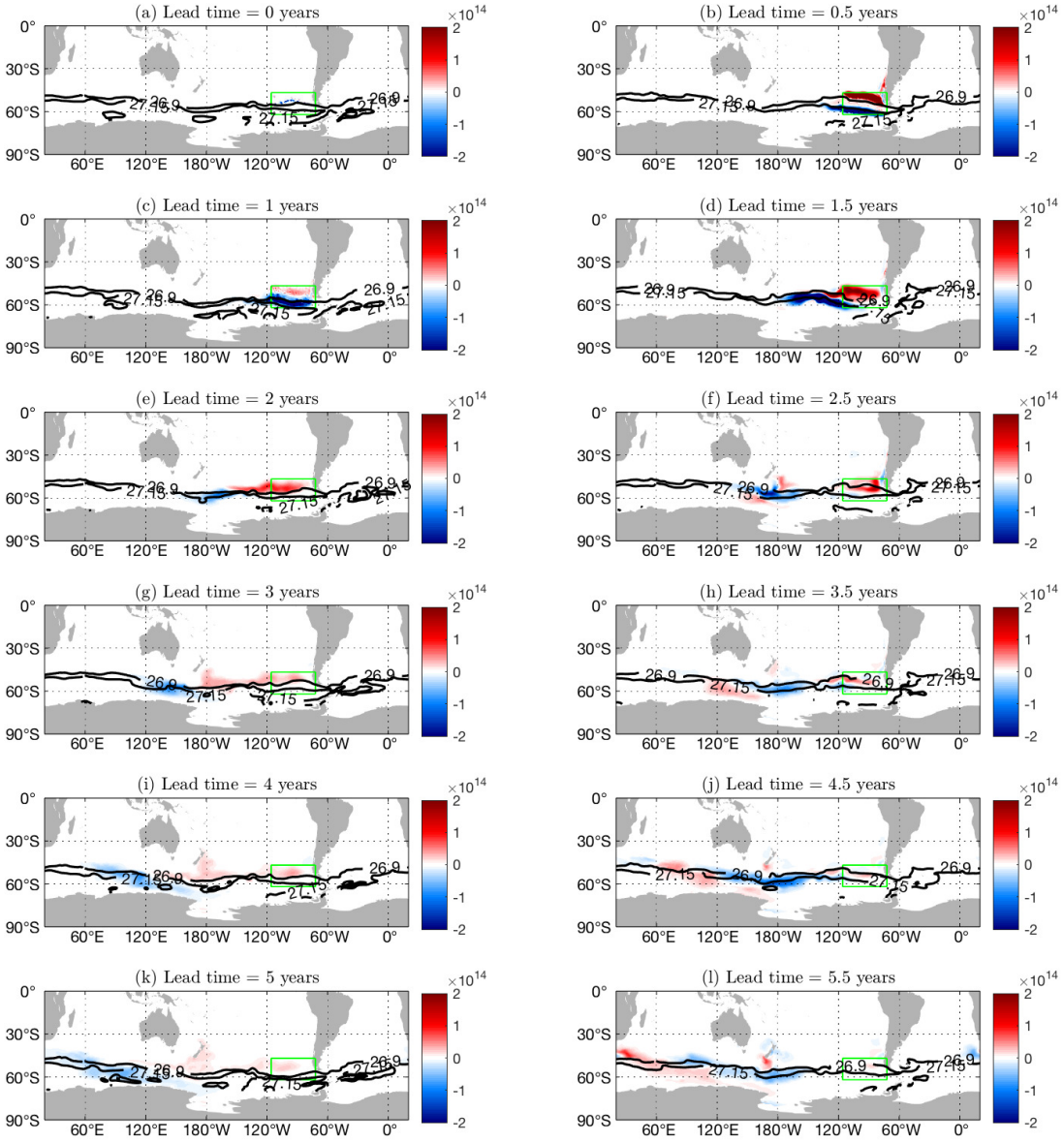

Figure S7. Surface heat flux impacts (m^3) at the surface for lead times of 0 - 5.5 years. The Eastern adjoint sensitivity target region (green) and the outcrops of the bounding density surfaces (26.9 and 27.15 kg m^{-3}, black contours) are included.

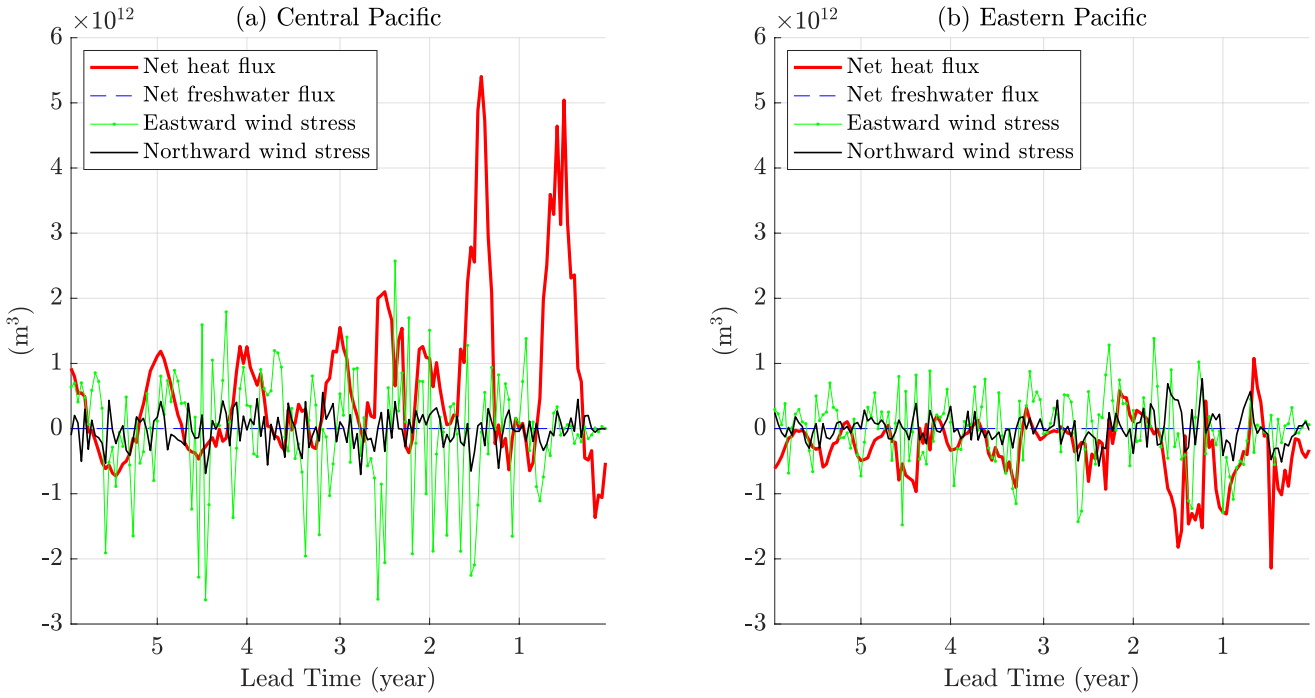

Figure S8. (a) Time series over lead time (year) of the total impacts of surface heat flux (sensitivity of volume to surface heat flux in the Central control volume multiplied by heat flux anomalies) (red thick, $m^{-1}\ s^{-1}$), eastward wind stress (green dotted, $m^{-1}\ s^{-1}$), northward wind stress (black thin, $m^{-1}\ s^{-1}$), and surface freshwater flux (blue dashed, $m^{-1}\ s^{-1}$). (b) Same for Eastern Pacific control volume.